The Astrophysical Journal, 670:1149–1158, 2007 December 1

SUPPRESSION OF PARTICLE DRIFTS BY TURBULENCE

J. Minnie,[1] J. W. Bieber, and W. H. Matthaeus
Bartol Research Institute, Department of Physics and Astronomy, 217 Sharp Laboratory, University of Delaware, Newark, DE 19716

and

R. A. Burger
Unit for Space Physics, School of Physics, Private Bag X6001, North-West University,
Potchefstroom Campus, Potchefstroom, 2520, South Africa
Received 2007 May 4; accepted 2007 July 31

ABSTRACT

We present results from direct numerical simulations showing the suppression of the large-scale drift motion of an ensemble of charged particles in a nonuniform turbulent magnetic field. We find that when scattering is negligible, the ensemble average drift velocity is in the direction predicted by the usual guiding center theory. When scattering is very strong, we find that all large-scale drift motions vanish. For an intermediate amount of scattering we find that the antisymmetric drift velocity is typically suppressed by a larger amount than the antisymmetric drift coefficient. We show that the total drift motion of the ensemble is not necessarily completely contained in the antisymmetric part of the diffusion tensor. Because of the occurrence of scattering, knowledge of the spatial variation of the symmetric part of the diffusion tensor is also needed to fully describe the total drift motion of the ensemble.

Subject headings: diffusion — turbulence

1. INTRODUCTION

It has long been known that large-scale drift plays an important role in the heliospheric modulation of cosmic rays (Jokipii et al. 1977). However, with the advent of more realistic numerical models of cosmic-ray modulation (Kóta & Jokipii 1983; Potgieter & Moraal 1985; Hattingh & Burger 1995), it soon became apparent that drift effects for low- to intermediate-energy cosmic rays should be suppressed to properly account for cosmic-ray observations (e.g., Potgieter et al. 1989).

From a simple hard-sphere scattering approach (e.g., Gleeson 1969) or using a velocity correlation function analysis (e.g., Bieber & Matthaeus 1997), one can see that the antisymmetric drift coefficient should be suppressed in the presence of scattering. Stawicki (2005) used a quasi-linear approach and showed that drifts are not reduced in the presence of unpolarized pure slab turbulence. The same conclusion was reached by Minnie (2006) based on numerical simulations similar to those reported in this paper, but using a different form for the nonuniform background magnetic field. Stawicki (2005) also considered the effect of composite slab/two-dimensional turbulence on drift, but since his turbulence includes a component aligned with the background field, in contrast to the purely transverse turbulence of the present study, a direct comparison should not be attempted. Various numerical studies have aimed to quantify the suppression of the antisymmetric drift coefficient (e.g., Giacalone et al. 1999; Candia & Roulet 2004). Although insightful, all previous numerical studies used models with a uniform large-scale magnetic field and scattering, making it impossible to relate the antisymmetric drift coefficient to the divergence of the antisymmetric diffusion tensor.

In order to relate the nonzero drift velocity $pv/(3q)\nabla \times \boldsymbol{B}/B^2$ to the nonzero drift coefficient $pv/(3qB)$, it is *required* that the magnetic field be spatially varying, otherwise the drift velocity is zero and any relation between the drift velocity and the drift coefficient is arbitrary. In the present study we use a nonuniform large-scale magnetic field in our numerical simulations to ensure that the large-scale drift velocity of the ensemble of particles is nonzero. We are therefore able for the first time to directly test the well-known relation between the large-scale drift velocity and large-scale drift coefficient and also study how these quantities are influenced by the occurrence of scattering. Preliminary results are presented in Minnie (2006) and are expanded on in the present study.

2. DRIFT THEORY

Charged particles moving in a nonuniform large-scale magnetic field will experience gradient and curvature drift. The well-known guiding center drift velocity of an ensemble of charged particles is given by (e.g., Rossi & Olbert 1970; Burger et al. 1985)

$$\boldsymbol{v}_D^{\rm ws} = \frac{pv}{3q}\nabla \times \frac{\boldsymbol{B}}{B^2}, \tag{1}$$

with p the relativistic particle momentum magnitude, v the particle speed, q the signed particle charge, and $\boldsymbol{B}$ the magnetic field. Note that this drift velocity can accommodate any variation in the large-scale field, but it does not include the effect of scattering, hence the superscript ws. Subsequently, the superscript ws is used to denote the weak-scattering limit of any particular quantity. Using a simple vector product identity, equation (1) can be written as

$$\boldsymbol{v}_D^{\rm ws} = \nabla \times \frac{pv}{3qB}\frac{\boldsymbol{B}}{B} = \nabla \times \kappa_A^{\rm ws}\boldsymbol{e}_B, \tag{2}$$

with $\boldsymbol{e}_B$ the unit vector along $\boldsymbol{B}$ and

$$\kappa_A^{\rm ws} \equiv \frac{pv}{3qB} = \frac{\beta P}{3B} = \frac{v}{3}r_M, \tag{3}$$

[1] Also at: Unit for Space Physics, School of Physics, Private Bag X6001, North-West University, Potchefstroom Campus, Potchefstroom, 2520, South Africa.

with $\beta = v/c$ the particle speed as a fraction of the speed of light, $P = pc/q$ the magnetic rigidity, and $r_M = P/(Bc)$ the maximal Larmor radius (i.e., 90° pitch angle). The quantity $\kappa_A^{\rm ws}$ is known as the weak-scattering drift coefficient.

The diffusion tensor used in heliospheric cosmic-ray modulation studies is (e.g., Gleeson 1969; Forman et al. 1974; Burger & Hattingh 1998)

$$\mathbf{K} = \begin{bmatrix} \kappa_\perp & \kappa_A & 0 \\ -\kappa_A & \kappa_\perp & 0 \\ 0 & 0 & \kappa_\parallel \end{bmatrix}, \tag{4}$$

with $\kappa_\perp$ and $\kappa_\parallel$ the diffusion coefficients perpendicular and parallel to the magnetic field, respectively, and κ_A the antisymmetric drift coefficient. This diffusion tensor can further be written as the sum of a symmetric part $\mathbf{K}^{(s)}$ containing the elements $\kappa_\perp$ and $\kappa_\parallel$ and an antisymmetric part $\mathbf{K}^{(a)}$ containing the element κ_A.

Cosmic-ray transport in the heliosphere is described by a Fokker-Planck equation (e.g., Parker 1965). The relevant term in the Fokker-Planck equation containing the diffusion tensor is

$$\nabla \cdot \left(\mathbf{K} \cdot \nabla U_p\right), \tag{5}$$

with U_p the differential particle density. Written out in full in index notation this term is

$$\kappa_{ij} \frac{\partial^2 U_p}{\partial x_i \partial x_j} + \frac{\partial \kappa_{ij}}{\partial x_i} \frac{\partial U_p}{\partial x_j}, \tag{6}$$

with κ_{ij} the diffusion tensor and summation over repeated indices is understood. Writing the diffusion tensor as the sum of a symmetric ($\kappa_{ij}^{(s)}$) and antisymmetric ($\kappa_{ij}^{(a)}$) part results in

$$\kappa_{ij}^{(s)} \frac{\partial^2 U_p}{\partial x_i \partial x_j} + \frac{\partial \kappa_{ij}^{(s)}}{\partial x_i} \frac{\partial U_p}{\partial x_j} + \underbrace{\kappa_{ij}^{(a)} \frac{\partial^2 U_p}{\partial x_i \partial x_j}}_{=0} + \frac{\partial \kappa_{ij}^{(a)}}{\partial x_i} \frac{\partial U_p}{\partial x_j}. \tag{7}$$

The third term is equal to zero due to the antisymmetry of κ_{ij}. The grouping of the remaining three terms can occur in two different ways. In the usual grouping, the terms containing the symmetric tensor are put together, namely,

$$\left(\kappa_{ij}^{(s)} \frac{\partial^2 U_p}{\partial x_i \partial x_j} + \frac{\partial \kappa_{ij}^{(s)}}{\partial x_i} \frac{\partial U_p}{\partial x_j}\right) + \frac{\partial \kappa_{ij}^{(a)}}{\partial x_i} \frac{\partial U_p}{\partial x_j}, \tag{8}$$

which can be written more compactly as

$$\frac{\partial}{\partial x_i}\left(\kappa_{ij}^{(s)} \frac{\partial U_p}{\partial x_j}\right) - v_j^{(a)} \frac{\partial U_p}{\partial x_j}, \tag{9}$$

with $\boldsymbol{v}^{(a)} \equiv -\nabla \cdot \mathbf{K}^{(a)}$. The association of the divergence of the (antisymmetric) diffusion tensor with a velocity is evident on dimensional grounds. The functional form and value of $\boldsymbol{v}^{(a)}$ follow from the observation that the divergence of an antisymmetric second-order tensor $\mathbf{A}$ can be written as the curl of a vector $\boldsymbol{a}$ (e.g., Aris 1989). Specifically, given that $\boldsymbol{a} = (a_1, a_2, a_3)$ and

$$\mathbf{A} = \begin{bmatrix} 0 & a_3 & -a_2 \\ -a_3 & 0 & a_1 \\ a_2 & -a_1 & 0 \end{bmatrix}, \tag{10}$$

it follows that

$$\nabla \times \boldsymbol{a} = -\nabla \cdot \mathbf{A}. \tag{11}$$

Substitution of $\mathbf{A}$ with $\mathbf{K}^{(a)}$ yields

$$\boldsymbol{v}^{(a)} = -\nabla \cdot \mathbf{K}^{(a)} = \nabla \times \kappa_A \boldsymbol{e}_B, \tag{12}$$

with $\boldsymbol{a} = (0, 0, \kappa_A)$ and the third directional component of $\boldsymbol{a}$ aligned with the direction of $\boldsymbol{e}_B$. For the case that $\kappa_A = \kappa_A^{\rm ws}$ (i.e., weak scattering), it follows from equation (2) that

$$-\nabla \cdot \mathbf{K}^{(a)} = \nabla \times \kappa_A^{\rm ws} \boldsymbol{e}_B = \boldsymbol{v}_D^{\rm ws}. \tag{13}$$

From these arguments it is evident that the coefficient in the antisymmetric part of the diffusion tensor is associated with large-scale drifts (Jokipii et al. 1977), and equation (9), as well as equation (5), takes on the familiar form

$$\nabla \cdot \left(\mathbf{K}^{(s)} \cdot \nabla U_p\right) - \boldsymbol{v}_D^{\rm ws} \cdot \nabla U_p, \tag{14}$$

when scattering is sufficiently weak.

However, equations (9) and (14) give the impression that it is only the antisymmetric tensor that is associated with large-scale drifts. The term containing the symmetric tensor also includes a divergence of that tensor, but it is not emphasized as is done for the antisymmetric tensor.

We find it more illuminating to rather group the two divergence terms in equation (7) together, namely,

$$\kappa_{ij}^{(s)} \frac{\partial^2 U_p}{\partial x_i \partial x_j} + \left(\frac{\partial \kappa_{ij}^{(s)}}{\partial x_i} + \frac{\partial \kappa_{ij}^{(a)}}{\partial x_i}\right) \frac{\partial U_p}{\partial x_j}, \tag{15}$$

which can be written more compactly as

$$\kappa_{ij}^{(s)} \frac{\partial^2 U_p}{\partial x_i \partial x_j} - v_j^{(\rm div)} \frac{\partial U_p}{\partial x_j}, \tag{16}$$

with $\boldsymbol{v}^{(\rm div)} = -\boldsymbol{v}^{(s)} + \boldsymbol{v}^{(a)} \equiv -\nabla \cdot (\mathbf{K}^{(s)} + \mathbf{K}^{(a)})$. The superscript (div) is to emphasize that the velocity under consideration is the result of taking the divergence of the full diffusion tensor $\mathbf{K}$. The different signs in the definitions of $\boldsymbol{v}^{(s)}$ and $\boldsymbol{v}^{(a)}$ are in anticipation of the results from the numerical simulations. The vectors $\boldsymbol{v}^{(s)}$ and $\boldsymbol{v}^{(a)}$ are therefore

$$\boldsymbol{v}^{(s)} \equiv +\nabla \cdot \mathbf{K}^{(s)} = \begin{bmatrix} \partial \kappa_\perp / \partial x \\ \partial \kappa_\perp / \partial y \\ \partial \kappa_\parallel / \partial z \end{bmatrix}, \tag{17}$$

$$\boldsymbol{v}^{(a)} \equiv -\nabla \cdot \mathbf{K}^{(a)} = \begin{bmatrix} \partial \kappa_A / \partial y \\ -\partial \kappa_A / \partial x \\ 0 \end{bmatrix}. \tag{18}$$

After grouping the two divergence terms together to obtain equation (16), it is now apparent that the effect of the spatial variation of the symmetric tensor stands on the same footing as the spatial variation of the antisymmetric tensor.

We choose to refer to $\boldsymbol{v}^{(s)}$ as *symmetric drift* and to $\boldsymbol{v}^{(a)}$ as *antisymmetric drift*, since these vectors are related to the divergence of the symmetric and antisymmetric diffusion tensors, respectively. There are also two key differences between these two velocities: (1) Symmetric drift is typically not divergence free,

while antisymmetric drift is divergence free by definition; and (2) symmetric drift is independent of particle charge, while antisymmetric drift is not.

Furthermore, it is clear that symmetric drift only occurs when nonuniform scattering is present. However, antisymmetric drift can occur in the absence of scattering, which yields nothing other than the classical weak-scattering drift value from equation (2). In the presence of scattering, antisymmetric drift is given by equation (12). It therefore remains to specify the antisymmetric coefficient κ_A that includes the effect of scattering.

Investigations of charged-particle transport based on isotropic scattering over some timescale τ (e.g., Gleeson 1969), quasi-linear treatment of particle streaming perpendicular to a large-scale magnetic field (e.g., Forman et al. 1974), or decorrelation of the particle velocities after some timescale τ (Bieber & Matthaeus 1997) all lead to the same functional form for the drift coefficient, namely,

$$\kappa_A = \frac{v}{3} r_M \frac{(\Omega\tau)^2}{1+(\Omega\tau)^2}. \tag{19}$$

Regardless of the model that is used to derive this drift coefficient, the result is always a quantity with a maximum value of $vr_M/3$ when $\Omega\tau \to \infty$ in the weak-scattering limit, and a minimum value of 0 when $\Omega\tau \to 0$ in the strong-scattering limit.

The formal structure of equation (19) should not be viewed as fundamental, except in the cited cases where it emerges rigorously. It should preferably be viewed as a parameterization of the suppression of the drift coefficient by turbulence. In particular, no reference is made to the specific physical effect that controls the timescale τ.

Therefore, without specifying $\Omega\tau$ we keep the drift coefficient general and write equation (19) as

$$\kappa_A \equiv \kappa_A^{\rm ws} f_s, \tag{20}$$

with $\kappa_A^{\rm ws} = vr_M/3$ (see eq. [3]) the weak-scattering value of the drift coefficient and $f_s = (\Omega\tau)^2/[1+(\Omega\tau)^2]$ the drift suppression factor due to the occurrence of scattering.

Following the analysis of Jokipii (1993) we use equation (20) in equation (12) to obtain

$$\begin{aligned} \boldsymbol{v}^{(a)} &\equiv -\nabla\cdot\mathbf{K}^{(a)} \\ &= \nabla\times\kappa_A\boldsymbol{e}_B \\ &= f_s\boldsymbol{v}_D^{\rm ws} + \nabla f_s\times\kappa_A^{\rm ws}\boldsymbol{e}_B, \end{aligned} \tag{21}$$

with $\boldsymbol{v}_D^{\rm ws} = \nabla\times\kappa_A^{\rm ws}\boldsymbol{e}_B$ (see eq. [2]).

The second term on the right-hand side of equation (21) can be neglected when scattering is either very strong or very weak. To see this, we write

$$\nabla f_s = \nabla\left[\frac{(\Omega\tau)^2}{1+(\Omega\tau)^2}\right] = \frac{2\Omega\tau\nabla(\Omega\tau)}{\left[1+(\Omega\tau)^2\right]^2}. \tag{22}$$

In the strong-scattering limit ($\Omega\tau \to 0$) we find

$$\lim_{\Omega\tau\to 0}\frac{\Omega\tau}{\left[1+(\Omega\tau)^2\right]^2} = \lim_{\Omega\tau\to 0}\Omega\tau = 0, \tag{23}$$

and in the weak-scattering limit ($\Omega\tau \to \infty$) we find

$$\lim_{\Omega\tau\to\infty}\frac{\Omega\tau}{\left[1+(\Omega\tau)^2\right]^2} = \lim_{\Omega\tau\to\infty}\frac{1}{(\Omega\tau)^3} = 0. \tag{24}$$

In these regimes of either strong or weak scattering, the only effect of the finite amount of scattering will be to suppress the antisymmetric drift coefficient and velocity by the same factor f_s (see eqs. [20] and [21]).

Furthermore, when scattering is strong ($\Omega\tau \to 0$) we see that the suppression factor f_s tends to zero, effectively nullifying the first term in equation (21) as well, resulting in the expected vanishing of the antisymmetric drift velocity in the presence of strong scattering. Thus, only when scattering is sufficiently weak are the nonzero antisymmetric drift coefficient and velocity suppressed by the same amount, that is,

$$\frac{\kappa_A}{\kappa_A^{\rm ws}} = \frac{\left|\boldsymbol{v}^{(a)}\right|}{\left|\boldsymbol{v}_D^{\rm ws}\right|} \equiv f_s. \tag{25}$$

For an intermediate amount of scattering we therefore see that the antisymmetric drift coefficient (eq. [20]) and total antisymmetric drift velocity (eq. [21]) do not have the same dependence on the suppression factor f_s, implying that these quantities might be influenced differently by the occurrence of scattering. In what follows we investigate this explicitly.

Note that up to this point we have implicitly assumed that the large-scale magnetic field is nonuniform. However, in the presence of scattering the full drift velocity is given by equation (21), and a nonuniform large-scale magnetic field is not necessarily needed for this velocity to be nonzero. With a uniform large-scale magnetic field, which will lead to $\boldsymbol{v}_D^{\rm ws} = 0$ (see eq. [2]), the presence of nonuniform scattering can still lead to antisymmetric drift (second term on the right-hand side of eq. [21]), which is similar in origin to symmetric drift (eq. [17]).

3. NUMERICAL EXPERIMENT DESIGN

In this section we describe the numerical experiment that is used to investigate the effects discussed in § 2. Generally in numerical simulations of this type, the large-scale magnetic field is uniform and the turbulence is statistically homogeneous (e.g., Giacalone & Jokipii 1994, 1999; Giacalone et al. 1999; Qin 2002; Candia & Roulet 2004; Minnie 2006). These two assumptions generally lead to no net drift in the numerical simulations. Although it is possible to determine the drift coefficient in a simulation in which the large-scale magnetic field is uniform (e.g., Giacalone et al. 1999; Candia & Roulet 2004; Minnie 2006), unless the scattering is nonuniform the first-order moments $\langle\Delta x\rangle/\Delta t$ and $\langle\Delta y\rangle/\Delta t$ will be zero. We aim to calculate these first-order moments directly and investigate their relationship to the drift coefficients explicitly.

To accomplish this, we use in our numerical simulations a nonuniform large-scale magnetic field, but still employ statistically homogeneous turbulence. The introduction of a nonuniform large-scale magnetic field has two effects. First, it leads to a large-scale drift velocity which is given by equation (2) when no scattering is present. Second, it gives rise to nonuniform scattering, since the ratio of the magnetic fluctuation amplitude to the magnitude of the large-scale magnetic field is now spatially varying. Scattering typically depends on this ratio.

The large-scale magnetic field is designed in a very specific way. Starting from equation (1), we write the weak-scattering drift velocity in terms of the magnetic rigidity $P \equiv pc/q$ as

$$\boldsymbol{v}_D^{\rm ws} = \frac{\beta P}{3} \nabla \times \frac{\boldsymbol{B}_{\rm ls}}{B_{\rm ls}^2}, \tag{26}$$

with $\beta = v/c$ the particle speed as a fraction of the speed of light c. We also add the subscript ls to the magnetic field vector and magnitude to denote that we are dealing with the large-scale magnetic field. We then choose the y-direction to be defined by the drift direction given by equation (26), the z-direction to be the direction along the large-scale magnetic field, and the x-direction to complete the Cartesian coordinate system. The drift speed in the y-direction in the absence of scattering is therefore

$$v_D^{\rm ws} = \frac{\beta P}{3} \frac{dB_{\rm ls}/dx}{B_{\rm ls}^2}. \tag{27}$$

This is the expression for the well-known gradient drift of charged particles in a nonuniform large-scale magnetic field, in the direction perpendicular to both the magnetic field and gradient direction. This drift speed clearly can be a function of position along the x-direction, and this spatial dependence varies depending on one's choice for the spatial dependence of the large-scale magnetic field.

To facilitate the calculation of the relevant ensemble averages in the numerical experiment, we require the drift speed (in the absence of scattering) given by equation (27) to be independent of position along the x-direction. In order to determine the required magnetic field, we rewrite the drift speed in equation (27) as

$$\frac{1}{B_{\rm ls}^2} \frac{dB_{\rm ls}}{dx} = \frac{3 v_D^{\rm ws}}{\beta P} = \mathcal{C}. \tag{28}$$

This equation can easily be solved to obtain the required magnetic field, namely,

$$B_{\rm ls}(x) = \frac{1}{a - \mathcal{C}x}, \tag{29}$$

with a an integration constant. We define the value B_0 to be that value of the magnetic field at $x = x_0$, where x_0 is the position at which the particles are injected along the x-direction. This leads to

$$B_{\rm ls}(x) = \frac{B_0}{1 - B_0 \mathcal{C}(x - x_0)}. \tag{30}$$

This magnetic field has the property that it depends on the required drift speed. If one requires that the drift speed be zero, then $\mathcal{C} = 0$ and the magnetic field becomes uniform. However, a nonzero value of the drift speed results in a magnetic field that varies in the x-direction. The nonuniformity of the magnetic field is therefore adjusted by the magnitude of $\mathcal{C}$.

A graphical representation of the large-scale magnetic field is shown in Figure 11. Here we show the magnetic field in the (x, z)-plane, where the length and direction of the arrows denote the magnitude and direction of the large-scale field, respectively. Furthermore, due to the spatial variation of the large-scale magnetic field, the gradient of $\delta B/B_{\rm ls}$ is in the negative x-direction, as indicated on this graph.

In order to determine the value of $\mathcal{C}$ to use in the simulations, we write

$$\mathcal{C} = \frac{3 v_D^{\rm ws}}{\beta P} = \frac{3}{B_0} \frac{v_D^{\rm ws}}{v} \frac{B_0 c}{P} = \frac{3}{B_0 \lambda_{\rm sl}} \frac{v_D^{\rm ws}}{v} \frac{\lambda_{\rm sl}}{r_M^0}, \tag{31}$$

with r_M^0 the maximal Larmor radius (i.e., particle with a 90° pitch angle) of the particles where $B_{\rm ls}(x) = B_0$. We also introduced the length scale $\lambda_{\rm sl}$, which is the bend-over scale of the slab turbulence (see eq. [36]) and acts as the unit of length in the simulations. We choose to fix the value of $v r_M^0 / v_D^{\rm ws} \lambda_{\rm sl} = 100$, implying

$$\frac{v_D^{\rm ws}}{v} = \frac{r_M^0/\lambda_{\rm sl}}{100}. \tag{32}$$

In the notation introduced in § 2, equation (32) is the antisymmetric drift velocity in the weak-scattering limit (see eq. [21]).

The simulation box is subsequently filled with a magnetic field which consists of the large-scale nonuniform component $\boldsymbol{B}_{\rm ls} = (0, 0, B_{\rm ls})$ and a statistically homogeneous randomly fluctuating component $\delta \boldsymbol{B} = (\delta B_x, \delta B_y, 0)$, which is transverse to the large-scale field. This random component of the magnetic field is further assumed to be a composite of two types of fluctuations, namely, slab and two-dimensional (2D) fluctuations. The energy distribution in the fluctuations is such that 20% of the total fluctuation energy resides in those fluctuations that vary in the direction along the background magnetic field (slab fluctuations) and the remaining 80% of the energy resides in fluctuations that vary in the plane perpendicular to the background magnetic field (2D fluctuations). This distribution of energy in the turbulent fluctuations is representative of solar wind conditions at Earth (Bieber et al. 1996) and is also in accord with previous numerical simulation studies (e.g., Giacalone & Jokipii 1999; Qin 2002; Shalchi 2005). The fluctuation vector is (e.g., Gray et al. 1996)

$$\delta \boldsymbol{B}(x, y, z) = \delta \boldsymbol{B}_{\rm sl}(z) + \delta \boldsymbol{B}_{\rm 2D}(x, y), \tag{33}$$

where $\delta \boldsymbol{B}_{\rm sl}$ represents the slab component and $\delta \boldsymbol{B}_{\rm 2D}$ the 2D component of the fluctuation. The time-independent but spatially varying magnetic field is therefore given by

$$\boldsymbol{B}(\boldsymbol{r}) = \boldsymbol{B}_{\rm ls} + \delta \boldsymbol{B}(\boldsymbol{r}), \tag{34}$$

with $\delta \boldsymbol{B}(\boldsymbol{r})$ the broadband spectrum of fluctuations represented by equation (33) and $\boldsymbol{r}$ the position vector. This magnetic field is obtained by specifying the spectrum of fluctuations in k-space, choosing random phases for the Fourier coefficients, and then transforming to real space by inverse fast Fourier transforms.

The size of the simulation box is $L_x \times L_y \times L_z = 100\lambda_{\rm sl} \times 100\lambda_{\rm sl} \times 10,000\lambda_{\rm sl}$, with $\lambda_{\rm sl}$ the bend-over scale of the slab turbulence power spectrum (see eq. [36]). The magnetic field is stored on separate 1D and 2D grids, from which the total 3D fluctuating magnetic field can be obtained through equation (33). To obtain the magnetic field at a position between grid points, linear interpolation is used.

The 1D grid that contains the slab turbulence has $N_z = 2^{22}$ points, and the 2D grid that contains the 2D turbulence has $N_x \times N_y = 2^{12} \times 2^{12}$ points. The smallest and largest excited wave modes in the simulations are chosen to be $k_{\rm min} = 2\pi/L$ and $k_{\rm max} = \pi N/L$, respectively, with N and L the appropriate values for the number of grid points and box dimension, respectively, in the x-, y-, or z-direction.

The composite (slab/2D) spectrum model for axisymmetric turbulence (cf. Matthaeus & Smith 1981; Bieber et al. 1994, 2004) that is used in the simulations is specified as

$$\mathrm{Tr}\left[P_{ij}^{\mathrm{sl}}(\boldsymbol{k})\right] + \mathrm{Tr}\left[P_{ij}^{\mathrm{2D}}(\boldsymbol{k})\right], \tag{35}$$

with

$$\mathrm{Tr}\left[P_{ij}^{\mathrm{sl}}(\boldsymbol{k})\right] \equiv P_{xx}^{\mathrm{sl}}(\boldsymbol{k}) + P_{yy}^{\mathrm{sl}}(\boldsymbol{k}) = C_{\mathrm{sl}}\left(1 + k_z^2\lambda_{\mathrm{sl}}^2\right)^{-5/6}\delta(k_x)\delta(k_y), \tag{36}$$

$$\mathrm{Tr}\left[P_{ij}^{\mathrm{2D}}(\boldsymbol{k})\right] \equiv P_{xx}^{\mathrm{2D}}(\boldsymbol{k}) + P_{yy}^{\mathrm{2D}}(\boldsymbol{k}) = C_{\mathrm{2D}}\left(1 + k_\perp^2\lambda_{\mathrm{2D}}^2\right)^{-5/6}\frac{\delta(k_z)}{k_\perp}, \tag{37}$$

where the superscripts sl and 2D denote the slab and 2D turbulence spectrum, respectively, and $\boldsymbol{k} = (k_x, k_y, k_z)$ is the 3D wavevector. The perpendicular wavenumber $k_\perp$ is given by $k_\perp = (k_x^2 + k_y^2)^{1/2}$. In equations (36) and (37), the slab and 2D bend-over scales λ_{sl} and λ_{2D} are defined, and the constants C_{sl} and C_{2D} are used to determine the magnitude of $\delta\boldsymbol{B}_{\mathrm{sl}}$ and $\delta\boldsymbol{B}_{\mathrm{2D}}$, respectively. The 2D bend-over scale λ_{2D} is taken to be smaller than the slab bend-over scale λ_{sl} (e.g., Robinson & Rusbridge 1971). Specifically, we choose $\lambda_{\mathrm{sl}} = 10\lambda_{\mathrm{2D}}$. The slab bend-over scale is used as the unit of length in the numerical simulations. All lengths are normalized to this value.

The amplitude of the fluctuations is characterized by the ratio $\delta B/B_0$, i.e., the value of $\delta B/B_{\mathrm{ls}}(x)$ at $x = x_0$. Note, however, that the ratio $\delta B/B_{\mathrm{ls}}(x)$ varies with position along the x-direction, owing to the variation of $B_{\mathrm{ls}}(x)$.

We then proceed to compute the trajectories of 1000 particles in many random realizations of the magnetic field by solving the Newton-Lorentz equation,

$$\frac{d}{dt}[\boldsymbol{v}(t)] = \frac{q}{\gamma m_0}\boldsymbol{v}(t) \times \boldsymbol{B}[\boldsymbol{r}(t)], \tag{38}$$

for each particle numerically, with $\boldsymbol{v}$ the particle velocity, γ the Lorentz factor, m_0 the particle rest mass, q the signed particle charge, and $\boldsymbol{B}$ the imposed magnetic field of the background plasma. The neglect of the electric field in equation (38) arises from the assumption that the background plasma is neutral and also that the Alfvén speed of this plasma is much less than the particle speed.

The particles are injected uniformly in configuration space on the (y, z)-plane at $x = x_0 = 2L_x/3$ with an isotropic initial velocity distribution. The trajectory of each particle is then followed for a time $t = 2000\lambda_{\mathrm{sl}}/v$.

Once the trajectories are computed, we calculate the antisymmetric drift coefficients and total drift velocity. The drift speeds in the x- and y-directions are calculated as $\langle\Delta x\rangle/\Delta t$ and $\langle\Delta y\rangle/\Delta t$, respectively. Following Giacalone et al. (1999) we calculate the antisymmetric drift coefficients as $\kappa_{ij} = \langle v_i\Delta r_j\rangle$, where v_i is the velocity component in the ith direction and Δr_j is the displacement in the jth direction. Here $\langle\ldots\rangle$ denotes an appropriate ensemble average. Below, we employ an average over different particle trajectories and realizations of the turbulence.

4. RESULTS

We present results here for a set of numerical simulations in which the ratio $\delta B/B_{\mathrm{ls}}$ is varied from 0.1 to 10 and the particle energy is chosen such that the ratio $r_M^0/\lambda_{\mathrm{sl}}$ takes on the values 0.1 and 1. In Figure 1 we show the temporal evolution of the drift coefficients from a typical run. The drift coefficients are normalized to the weak-scattering value of the drift coefficient at $x = x_0$, namely, $vr_M^0/3$. Furthermore, we show moving averages superimposed on the data to better display the underlying trend. We believe the variation in the data to be the result of our sampling of the trajectories of only $\sim$5 times per gyroperiod. Eventually, we will only be concerned with the asymptotic value of the drift coefficient, which seems to be adequately described by the temporal average of the entire data set, as suggested by the moving average.

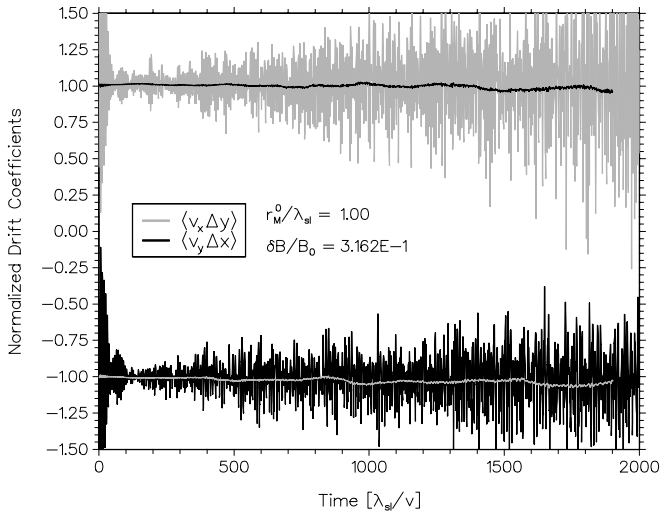

FIG. 1.—Drift coefficients $\langle v_y\Delta x\rangle$ (*bottom*) and $\langle v_x\Delta y\rangle$ (*top*) as a function of time for the case when $\delta B/B_0 = 0.3162$ and $r_M^0/\lambda_{\mathrm{sl}} = 1.0$, normalized to the weak-scattering value $vr_M^0/3$. Here r_M^0 is the maximal Larmor radius when $B = B_0$ at $x = x_0$, and λ_{sl} is the bend-over scale of the slab turbulence power spectrum. The smooth lines are moving averages to show the trend of the data.

We define the antisymmetric drift coefficient κ_A to be

$$\kappa_A \equiv \frac{\left|\overline{\kappa}_{xy}\right| + \left|\overline{\kappa}_{yx}\right|}{2}, \tag{39}$$

where the values $\overline{\kappa}_{yx}$ and $\overline{\kappa}_{xy}$ are the temporal averages of the data as shown in Figure 1. For an estimate of the uncertainty in κ_A, we use the deviation of $\overline{\kappa}_{yx}$ and $\overline{\kappa}_{xy}$ from pure antisymmetry. We define this deviation from antisymmetry σ_A as

$$\sigma_A \equiv \frac{\overline{\kappa}_{xy} + \overline{\kappa}_{yx}}{\overline{\kappa}_{xy} - \overline{\kappa}_{yx}}. \tag{40}$$

Therefore, when $\overline{\kappa}_{xy} \neq -\overline{\kappa}_{yx}$ then $\sigma_A \neq 0$ and the estimate for uncertainty in κ_A is then specified as $\epsilon_A \equiv \kappa_A\sigma_A$.

In Figures 2 and 3 we show the temporal evolution of the drift speed in the x- and y-directions, respectively, from a typical run. In these graphs, as well as in all subsequent presentations of the drift speeds, both speeds are normalized to the weak-scattering value of the drift speed in the y-direction, i.e., equation (32). Again, as in Figure 1, we are interested in the asymptotic values of these quantities. However, unlike the drift coefficients, the asymptotic regime is always preceded by some startup transient. We neglect this transient in our later presentations of the drift speeds and only consider the asymptotic value.

In Figures 4 and 5 we show the antisymmetric drift coefficient κ_A (see eqs. [39] and [40]) as a function of magnetic fluctuation amplitude, normalized to the weak-scattering value $vr_M^0/3$, for

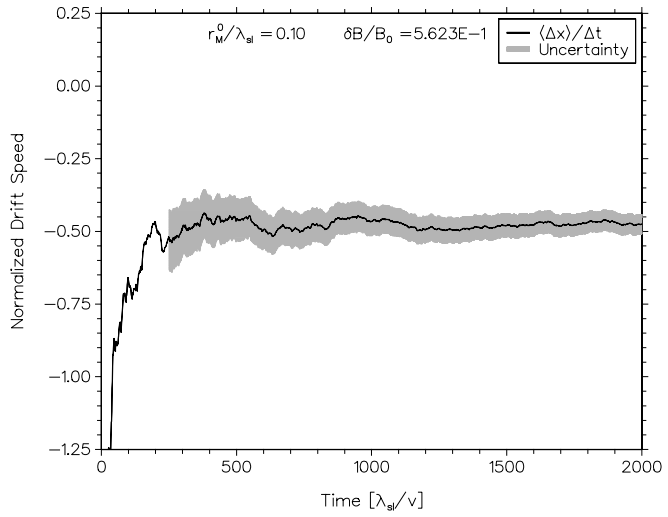

FIG. 2.—Drift speed in the x-direction as a function of time normalized to the weak-scattering value of the drift speed in the y-direction, for the case when $\delta B/B_0 = 0.5623$ and $r_M^0/\lambda_{sl} = 0.1$. The gray shaded region denotes the uncertainty in the drift speed, arising from the ensemble-averaging process.

the two cases $r_M^0/\lambda_{sl} = 1.0$ and $r_M^0/\lambda_{sl} = 0.1$, respectively. Here $r_M^0 = P/(B_0 c)$ is the maximal Larmor radius when $B = B_0$ at $x = x_0$, and λ_{sl} is the bend-over scale of the slab turbulence power spectrum (see eq. [36]).

In each respective graph, results from two different simulations are shown: one set of simulations in which the large-scale magnetic field is uniform (Minnie 2006) and the present set of simulations in which the large-scale magnetic field is nonuniform. The good agreement between the results from the two different sets of simulations suggests that simulations in which the large-scale magnetic field is uniform are sufficient to determine the drift coefficient. That is, the magnitude of the drift coefficient is independent of the structure of the large-scale field and only requires the magnitude of the magnetic field to be known. Furthermore, the values for the antisymmetric drift coefficient lie between the weak-scattering value and zero as equation (19) predicts, and these values remain close to or at the weak-scattering value for larger values of $\delta B/B_0$ when the rigidity is higher.

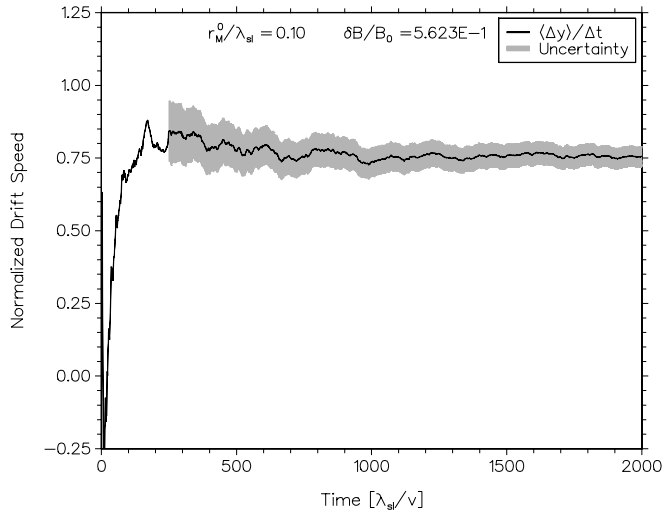

FIG. 3.—Drift speed in the y-direction as a function of time normalized to the weak-scattering value of the drift speed in the same direction, for the case when $\delta B/B_0 = 0.5623$ and $r_M^0/\lambda_{sl} = 0.1$. The gray shaded region denotes the uncertainty in the drift speed, arising from the ensemble-averaging process.

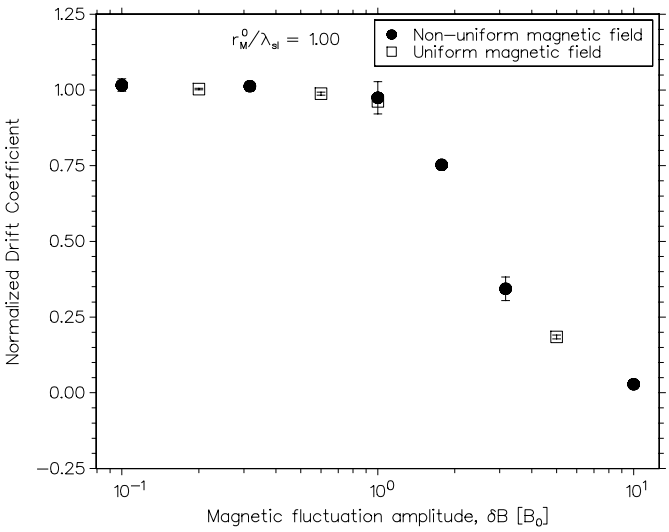

FIG. 4.—Drift coefficient κ_A as a function of magnetic fluctuation amplitude, normalized to the weak-scattering value $vr_M^0/3$. Here r_M^0 is the maximal Larmor radius when $B = B_0$ at $x = x_0$. The filled circles are simulation results using a magnetic field with a nonuniform large-scale component, while the open squares are simulation results using a magnetic field with a uniform large-scale component. All simulations are performed for $r_M^0/\lambda_{sl} = 1.0$, with λ_{sl} the bend-over scale of the slab turbulence power spectrum.

In Figures 6 and 7 we show the drift speed in the x-direction ($\langle \Delta x \rangle / \Delta t$) as a function of magnetic fluctuation amplitude, normalized to the weak-scattering value of the drift speed in the y-direction (eq. [32]), for the two cases $r_M^0/\lambda_{sl} = 1.0$ and $r_M^0/\lambda_{sl} = 0.1$, respectively. Again, as presented in Figures 4 and 5, we show a set of simulation results using a uniform large-scale magnetic field (Minnie 2006) and the set of simulations from the present study using a nonuniform large-scale magnetic field. Clearly, for the case of a uniform large-scale magnetic field, the displacements Δx average to zero and therefore the drift speed is zero. However, when the large-scale magnetic field is nonuniform, the displacements Δx do not average to zero, and this results in net drift in the x-direction.

This drift motion in the x-direction cannot be accounted for by equation (21), because it is in the same direction as the gradient in the field. This drift speed can therefore not be associated with the antisymmetric drift coefficient. Instead, since the spatial variation

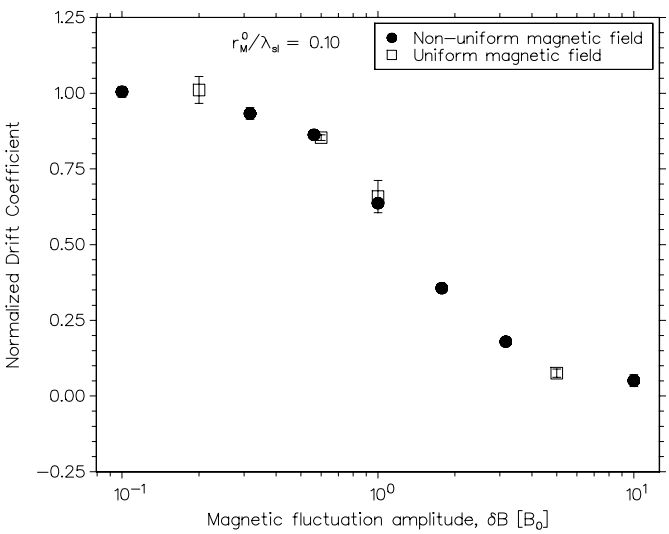

FIG. 5.—Same as Fig. 4, but for $r_M^0/\lambda_{sl} = 0.1$.

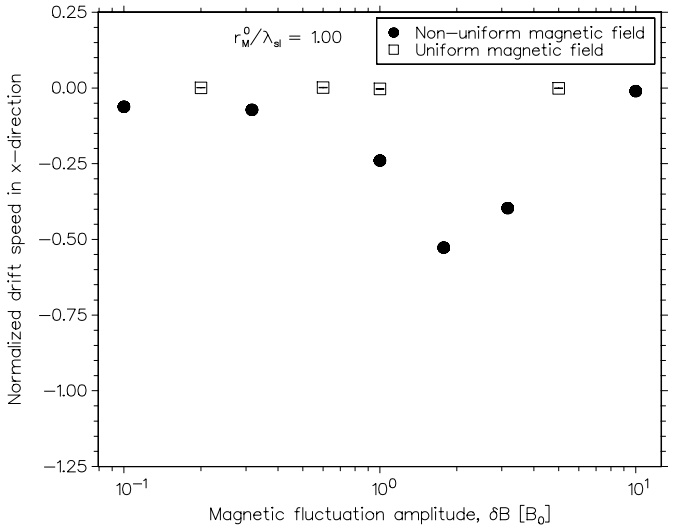

FIG. 6.—Drift speed in the x-direction as a function of magnetic fluctuation amplitude, normalized to the weak-scattering value of the drift speed in the y-direction (eq. [32]). The filled circles are simulation results using a magnetic field with a nonuniform large-scale component, while the open squares are simulation results using a magnetic field with a uniform large-scale component. All simulations are performed for $r_M^0/\lambda_{\rm sl} = 1.0$, with r_M^0 the maximal Larmor radius when $B = B_0$ at $x = x_0$ and $\lambda_{\rm sl}$ the bend-over scale of the slab turbulence power spectrum.

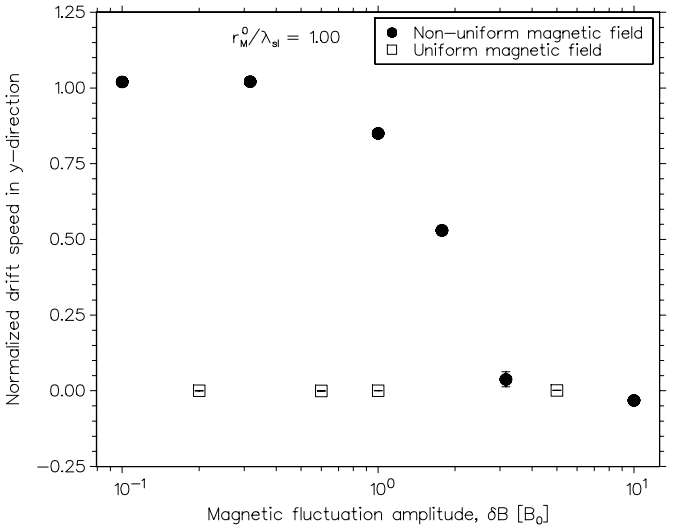

FIG. 8.—Drift speed in the y-direction as a function of magnetic fluctuation amplitude, normalized to the weak-scattering value of the drift speed in the same direction (eq. [32]). The filled circles are simulation results using a magnetic field with a nonuniform large-scale component, while the open squares are simulation results using a magnetic field with a uniform large-scale component. All simulations are performed for $r_M^0/\lambda_{\rm sl} = 1.0$, with r_M^0 the maximal Larmor radius when $B = B_0$ at $x = x_0$ and $\lambda_{\rm sl}$ the bend-over scale of the slab turbulence power spectrum.

in the simulations is in the x-direction only, we see from equations (17) and (18) that the velocities $\boldsymbol{v}^{(s)}$ and $\boldsymbol{v}^{(a)}$ are

$$\boldsymbol{v}^{(s)} = (\partial\kappa_\perp/\partial x, 0, 0), \quad \boldsymbol{v}^{(a)} = (0, -\partial\kappa_A/\partial x, 0) \qquad (41)$$

in a Cartesian coordinate system. It is therefore evident that this drift motion in the x-direction is related to the spatial variation of the perpendicular diffusion coefficient (i.e., the divergence of the symmetric part of the diffusion tensor) and does not involve the antisymmetric drift coefficient κ_A.

To see that these velocities are in the appropriate directions, we note from numerical simulations (e.g., Giacalone & Jokipii 1999; Minnie 2006; Minnie et al. 2007) and analytical considerations (e.g., Jokipii 1966; Matthaeus et al. 2003; Shalchi et al. 2004) that the perpendicular diffusion coefficient scales with the ratio $\delta B/B_{\rm ls}$. From the simulations of the present study, this implies $\partial\kappa_\perp/\partial x < 0$ (cf. Fig. 11), which is stating that symmetric drift is in the negative x-direction. This is consistent with the simulations shown in Figures 6 and 7.

Finally, we present the gradient drift speed which is of course in the y-direction and therefore perpendicular to both the large-scale magnetic field direction and the direction of the gradient in the large-scale magnetic field. In Figures 8 and 9 we show the drift speed in the y-direction ($\langle\Delta y\rangle/\Delta t$) as a function of magnetic fluctuation amplitude, normalized to the weak-scattering value of the drift speed in the same direction (eq. [32]), for the two cases $r_M^0/\lambda_{\rm sl} = 1.0$ and $r_M^0/\lambda_{\rm sl} = 0.1$, respectively.

For the expected direction of antisymmetric drift we note that in the weak-scattering limit at least, the drift coefficient is inversely proportional to the large-scale magnetic field. This implies from the current simulations that $\partial\kappa_A^{\rm ws}/\partial x < 0$, which means that the direction of the antisymmetric drift velocity is in the positive

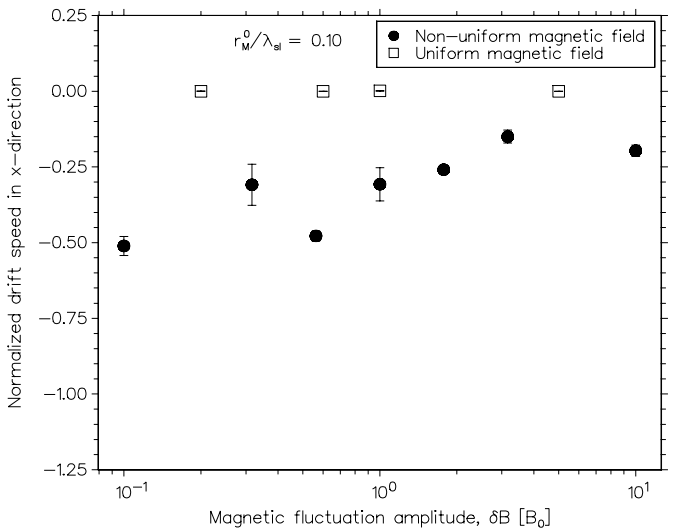

FIG. 7.—Same as Fig. 6, but for $r_M^0/\lambda_{\rm sl} = 0.1$.

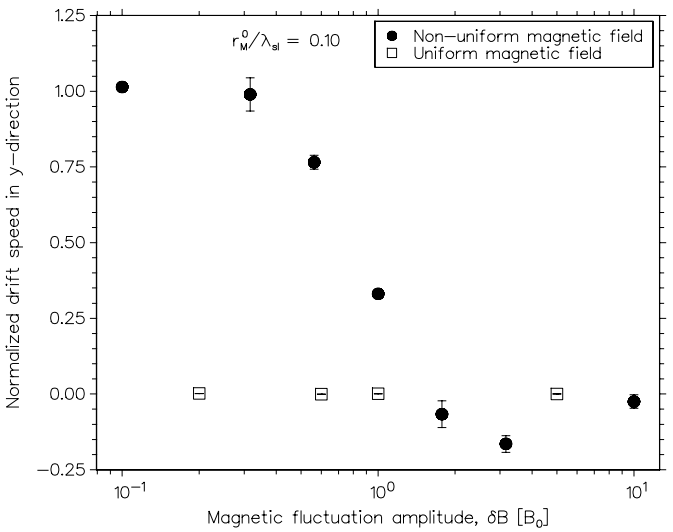

FIG. 9.—Same as Fig. 8, but for $r_M^0/\lambda_{\rm sl} = 0.1$.

y-direction. This is also consistent with the simulations shown in Figures 8 and 9 when $\delta B/B_{\rm ls}$ is sufficiently small. When $\delta B/B_{\rm ls}$ becomes sufficiently large and the antisymmetric drift direction changes, we believe that the entire system becomes diffusion-dominated, rather than drift-dominated, leading to drift which is similar in origin to that of symmetric drift.

Again, as discussed for drift in the x-direction, the simulations using a uniform large-scale magnetic field lead to no net drift, since the scattering merely randomizes the displacements which end up averaging to zero. However, with the nonuniform large-scale magnetic field, the particles drift in the y-direction, and this drift is scaled down with respect to the weak-scattering value when the magnetic fluctuation amplitude becomes sufficiently large. Furthermore, similar to the drift coefficient in Figures 4 and 5, the drift speed is scaled down differently for particles of different rigidities.

We note first the apparent change of drift direction when the magnetic fluctuation amplitude becomes large. This is especially visible in Figure 9, for the case $r_M^0/\lambda_{\rm sl} = 0.1$. This change of drift direction emphasizes the importance of the second term in equation (21), since the first term cannot account for the change in drift direction. Second, we observe that the drift speed is always reduced more than the drift coefficient of the same rigidity (cf. Figs. 4 and 8 and Figs. 5 and 9). To quantify this difference in suppression, we rearrange equation (21) and define the *residual antisymmetric drift velocity* as

$$\boldsymbol{v}_R^{(a)} \equiv \nabla f_s \times \kappa_A^{\rm ws} \boldsymbol{e}_B = \nabla \times \kappa_A \boldsymbol{e}_B - f_s \boldsymbol{v}_D^{\rm ws}. \tag{42}$$

Because of the design of the numerical experiment these quantities are all oriented in the y-direction. Specializing to the y-direction we obtain

$$v_R^{(a)} = -\frac{\partial \kappa_A}{\partial x} - f_s v_D^{\rm ws}. \tag{43}$$

The first term on the right-hand side of this equation is the total antisymmetric drift speed $\left|\boldsymbol{v}^{(a)}\right|$ in the y-direction (see eq. [21]) given by $\langle \Delta y \rangle / \Delta t$ in the simulations. We can therefore normalize this equation to the weak-scattering drift speed in the y-direction to obtain

$$\tilde{v}_R^{(a)} = \tilde{v}^{(a)} - f_s, \tag{44}$$

where the tilde denotes normalization by $v_D^{\rm ws}$. If we finally choose f_s to be given by $\kappa_A/\kappa_A^{\rm ws}$ (see eq. [25]) from the simulations, we effectively define the difference by which the antisymmetric drift coefficient and total antisymmetric drift velocity is suppressed.

In Figure 10 we show the normalized residual antisymmetric drift speed $\tilde{v}_R^{(a)}$ from the simulations. Note that $\tilde{v}_R^{(a)}$ tends to zero when the amplitude of the fluctuations becomes very small or very large. This is in agreement with the analytical calculations performed in equations (23) and (24) where it is shown that this residual drift velocity should go to zero when scattering is very strong or very weak. Furthermore, at intermediate values for $\delta B/B_0$ the antisymmetric drift velocity can be suppressed by up to $\sim$45% *more* than the antisymmetric drift coefficient.

It is intuitively reasonable to expect that this residual drift can be either in the same or opposite direction as the antisymmetric drift velocity. This property is of interest to determine whether the drift coefficient is suppressed by the same amount as, more than, or less than the antisymmetric drift velocity with which it is related. From the present simulations we consistently find that the antisymmetric drift velocity is suppressed more than the antisymmetric drift coefficient. Whether this is generally true is still an open question.

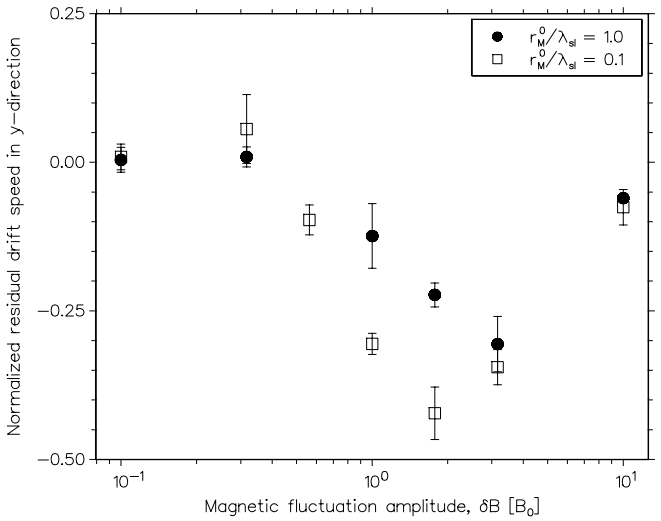

FIG. 10.—Residual antisymmetric drift speed in the y-direction for $r_M^0/\lambda_{\rm sl} = 1.0$ and $r_M^0/\lambda_{\rm sl} = 0.1$. The residual is normalized to the weak-scattering value of the drift speed in the y-direction.

5. DISCUSSION AND CONCLUSION

In Figure 12 we show a schematic representation of all the drift motions that can occur in the simulations of the present study. All the drift motions are in the (x, y)-plane (the plane of the paper), with the z-direction pointing outward. In conjunction with Figure 11 showing the geometry of the magnetic field, we discuss the following drift motions:

Classical gradient drift.—Starting from point A, positively charged particles will spiral into region L (to the left of the vertical dashed line) where their Larmor radii will become larger due to the decreasing large-scale magnetic field. After crossing the dashed line and entering region R, their Larmor radii will decrease due to the increasing large-scale magnetic field and the net motion from A to B is the result. Negatively charged particles, with the opposite sense of gyration, will drift in the opposite direction. In the absence of scattering this is the usual drift velocity known as the classical or weak-scattering drift velocity ($\boldsymbol{v}_D^{\rm ws}$). In the nomenclature of the present study this motion is given by equation (1) or (2).

Antisymmetric drift.—The full antisymmetric drift motion is comprised of two components. The one component is the classical gradient drift (discussed above) that is modified by the suppression factor f_s. The origin for the reduction of the classical drift velocity is just the presence of scattering. This is the first term on the right-hand side of equation (21). The other component of the antisymmetric drift is related to the gradient in scattering efficiency. When the particles find themselves in region L where the ratio $\delta B/B_{\rm ls}$ is large, more perpendicular diffusion is taking place than when the particles venture into region R where $\delta B/B_{\rm ls}$ is smaller. At any given point in region L and another point in region R, perpendicular diffusion is uniform in the y-direction, but occurring at different rates. This is denoted by the symmetric distributions with different widths in region L (wider due to more perpendicular diffusion) and R (narrower due to less perpendicular diffusion). The particle trajectories are therefore less perturbed in region R than in region L, leading to net motion in the negative y-direction ($\nabla f_s \times \kappa_A^{\rm ws} \boldsymbol{e}_B$). This is the origin of the change of drift direction seen in Figures 8 and 9.

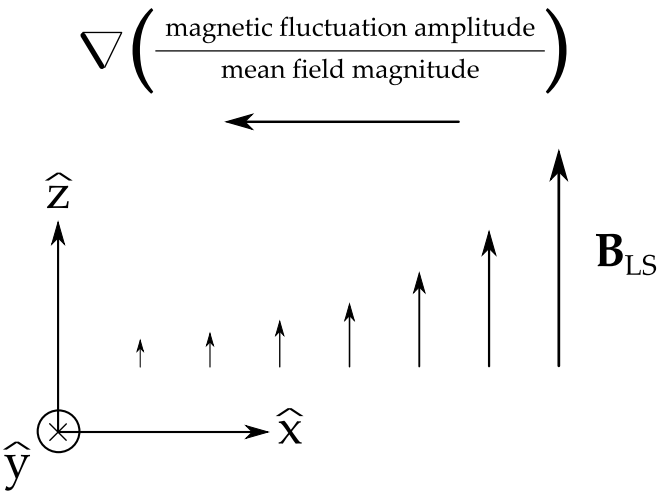

FIG. 11.—Magnetic field geometry used in the numerical simulations.

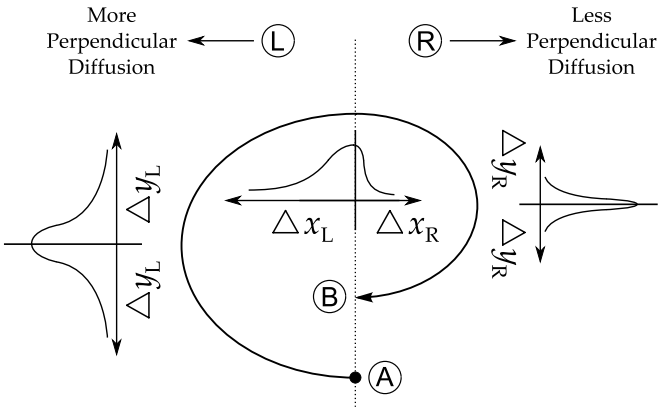

FIG. 12.—Particle orbit from point A to point B depicts the origin of classical (antisymmetric) gradient drift. The Gaussian distributions at left and right display the source of residual antisymmetric drift. Finally, the asymmetric distribution in the center depicts the origin of symmetric drift arising from the nonuniform perpendicular diffusion coefficient. See text for further details.

Another way to look at this is in terms of the parameterization of equation (19). Our simulations suggest that the suppression factor f_s increases to the right in Figure 12, because $\delta B/B_{ls}$ decreases in this direction. Thus, from this formal parameterization, $\Omega\tau$ approaches the weak-scattering limit toward the right. Noting that the large-scale magnetic field points out of the page (cf. Fig. 11), this gradient in scattering implies drift in the negative y-direction, as observed (cf. Jokipii 1993).

Symmetric drift.—Because of gradient in perpendicular diffusion along the x-direction, with the occurrence of more diffusion in region L than in region R, particles will spread more efficiently in region L than in region R. This leads to the skewed distribution shown in the middle of Figure 12; this argument holds for any given position. The tail of the distribution is longer in the direction where diffusion is more rapid, therefore resulting in the net migration of particles in the negative x-direction. This is what we have referred to as the symmetric drift velocity, since it is related to the divergence of the symmetric part of the diffusion tensor (see eq. [17]).

In the present study we have shown by means of direct numerical simulations that the large-scale antisymmetric drift velocity of an ensemble of particles is suppressed with respect to the expected weak-scattering value in the presence of sufficiently strong magnetic turbulence. We have shown that only in the limiting cases of either very strong or very weak turbulence are the antisymmetric drift coefficient and the antisymmetric drift velocity suppressed by an equal amount. For the more general case of intermediate turbulence we have shown that the antisymmetric drift velocity is suppressed more than the antisymmetric drift coefficient, and under certain conditions, it is even possible for the antisymmetric drift velocity to change direction.

Our discussion of a second kind of drift motion that we have classified as symmetric drift should not be taken as a claim of discovery of some new effect that should be included in future transport models. We understand that this is already included through the usual divergence of the symmetric diffusion tensor. We merely wish to emphasize that the drift motion of an ensemble of particles is not necessarily completely contained in the antisymmetric part of the diffusion tensor. To understand the full drift motion of an ensemble of particles one must have knowledge of the spatial variation of the symmetric part of the diffusion tensor as well.

Finally, it is interesting to note that the regime where antisymmetric drift seems to be changing from its weak-scattering value to some suppressed value broadly corresponds with the range where the magnetic fluctuation amplitude is comparable to the background magnetic field magnitude. The case of $\delta B/B_{ls} \sim 1$ is quite characteristic of the solar wind, especially at Earth (e.g., see Fig. 4*c* of Bieber et al. 1993), and it would seem that the region where we find the most variation in the antisymmetric drift velocity is in that region of observed magnetic fluctuation amplitudes in interplanetary space.

This work was supported by NASA grant NNX 07-AH73G. R. A. B. acknowledges support by the South African National Research Foundation.

REFERENCES

Aris, R. 1989, Vectors, Tensors, and the Basic Equations of Fluid Mechanics (New York: Dover)
Bieber, J. W., Chen, J., Matthaeus, W. H., Smith, C. W., & Pomerantz, M. A. 1993, J. Geophys. Res., 98, 3585
Bieber, J. W., & Matthaeus, W. H. 1997, ApJ, 485, 655
Bieber, J. W., Matthaeus, W. H., Shalchi, A., & Qin, G. 2004, Geophys. Res. Lett., 31, 10805
Bieber, J. W., Matthaeus, W. H., Smith, C. W., Wanner, W., Kallenrode, M.-B., & Wibberenz, G. 1994, ApJ, 420, 294
Bieber, J. W., Wanner, W., & Matthaeus, W. H. 1996, J. Geophys. Res., 101, 2511
Burger, R. A., & Hattingh, M. 1998, ApJ, 505, 244
Burger, R. A., Moraal, H., & Webb, G. M. 1985, Ap&SS, 116, 107
Candia, J., & Roulet, E. 2004, J. Cosmol. Astropart. Phys., 10, 7
Forman, M. A., Jokipii, J. R., & Owens, A. J. 1974, ApJ, 192, 535
Giacalone, J., & Jokipii, J. R. 1994, ApJ, 430, L137
———. 1999, ApJ, 520, 204
Giacalone, J., Jokipii, J. R., & Kóta, J. 1999, in Proc. 26th Int. Cosmic Ray Conf. (Salt Lake City), 37
Gleeson, L. J. 1969, Planet. Space Sci., 17, 31
Gray, P. C., Pontius, D. H., Jr., & Matthaeus, W. H. 1996, Geophys. Res. Lett., 23, 965
Hattingh, M., & Burger, R. A. 1995, Adv. Space Res., 16, 213
Jokipii, J. R. 1966, ApJ, 146, 480
———. 1993, in Proc. 23rd Int. Cosmic Ray Conf. (Calgary), 497
Jokipii, J. R., Levy, E. H., & Hubbard, W. B. 1977, ApJ, 213, 861
Kóta, J., & Jokipii, J. R. 1983, ApJ, 265, 573
Matthaeus, W. H., Qin, G., Bieber, J. W., & Zank, G. P. 2003, ApJ, 590, L53

Matthaeus, W. H., & Smith, C. 1981, Phys. Rev. A, 24, 2135
Minnie, J. 2006, Ph.D. thesis, North-West Univ. (Potchefstroom)
Minnie, J., Bieber, J. W., Matthaeus, W. H., & Burger, R. A. 2007, ApJ, 663, 1049
Parker, E. N. 1965, Planet. Space Sci., 13, 9
Potgieter, M. S., le Roux, J. A., & Burger, R. A. 1989, J. Geophys. Res., 94, 2323
Potgieter, M. S., & Moraal, H. 1985, ApJ, 294, 425
Qin, G. 2002, Ph.D. thesis, Univ. Delaware
Robinson, D. C., & Rusbridge, M. G. 1971, Phys. Fluids, 14, 2499
Rossi, B., & Olbert, S. 1970, Introduction to the Physics of Space (New York: McGraw-Hill)
Shalchi, A. 2005, MNRAS, 363, 107
Shalchi, A., Bieber, J. W., & Matthaeus, W. H. 2004, ApJ, 604, 675
Stawicki, O. 2005, ApJ, 624, 178